Ultrafast valley relaxation dynamics in monolayer MoS$_2$ probed by nonequilibrium optical techniques

S. Dal Conte,[1,2] F. Bottegoni,[2] E. A. A. Pogna,[2] D. De Fazio,[3] S. Ambrogio,[4] I. Bargigia,[5] C. D'Andrea,[2,5] A. Lombardo,[3] M. Bruna,[3] F. Ciccacci,[2] A. C. Ferrari,[3] G. Cerullo,[1,2] and M. Finazzi[2]

[1]*IFN-CNR, Piazza L. da Vinci 32, I-20133 Milano, Italy*
[2]*Dipartimento di Fisica, Politecnico di Milano, Piazza L. da Vinci 32, I-20133 Milano, Italy*
[3]*Cambridge Graphene Centre, University of Cambridge, 9 JJ Thomson Avenue, Cambridge CB3 0FA, United Kingdom*
[4]*Dipartimento di Elettronica, Informatica e Bioingegneria, Politecnico di Milano and IU.NET, I-20133 Milano, Italy*
[5]*Center for Nano Science and Technology @PoliMi, Istituto Italiano di Tecnologia, via Giovanni Pascoli 70/3, 20133 Milan, Italy*

We study the exciton valley relaxation dynamics in single-layer MoS$_2$ by a combination of two nonequilibrium optical techniques: time-resolved Faraday rotation and time-resolved circular dichroism. The depolarization dynamics, measured at 77 K, exhibits a peculiar biexponential decay, characterized by two distinct time scales of 200 fs and 5 ps. The fast relaxation of the valley polarization is in good agreement with a model including the intervalley electron-hole Coulomb exchange as the dominating mechanism. The valley relaxation dynamics is further investigated as a function of temperature and photoinduced exciton density. We measure a strong exciton density dependence of the transient Faraday rotation signal. This indicates the key role of exciton-exciton interactions in MoS$_2$ valley relaxation dynamics.

I. INTRODUCTION

Exploiting and manipulating the spin and valley degrees of freedom in order to process and store information is one of the most challenging goals of modern solid-state physics, and already resulted in the demonstration of several functional devices [1–6]. In this context, transition metal dichalcogenides (TMDs) add novel functionalities, due to the strong interplay between the spin and the crystal momentum of the carriers [7], and represent a promising platform to develop new spin and valleytronic devices thanks to their peculiar electronic structure [8] and the integrability with graphene technology [9,10].

In a single MoS$_2$ layer (1L-MoS$_2$) both the minimum of the conduction band (CB) and the maximum of the valence band (VB) are located at the **K** and **K$'$** points of the Brillouin zone [11,12], allowing for direct absorption transitions in the visible range [13]. The lack of inversion symmetry, combined with the C_{3h} symmetry of the Bloch wave functions at **K**, **K$'$**, leads to electron states with a nonvanishing projection of their average angular momentum $\langle L_z \rangle$ along the direction perpendicular to the MoS$_2$ plane [11,12]. In particular, at **K**, the CB minimum and the VB maximum are mainly composed of Mo d orbitals with $m = 0$ and $m = 2$, respectively. At **K$'$** the signs are inverted, since **K**, **K$'$** are related to each other by time-reversal conjugation [11,12,14]. The valley index can be thus regarded as a discrete degree of freedom for low-energy carriers, robust against defects, contaminants, and low-energy phonons, because of the large valley separation in momentum space [15], in principle enabling valley-based noise-resistant quantum computation [16].

The strong spin-orbit interaction acting on the d-derived states with $m = 2$ at the VB maximum induces a $\Delta E_{SO} = 160$-meV energy split between spin-up and spin-down states, and determines opposite spin polarizations at the VB **K**, **K$'$** [Fig. 1(a)] [11,12]. Conversely, $\langle L_z \rangle$ at the CB minima has a

small contribution from the p atomic orbitals of the chalcogen (S) atoms (see Table II in Ref. [11]), resulting in a small spin-orbit splitting (a few meV) [11,12]. States with opposite spins at the bottom of the CB band are thus almost degenerate, meaning that the spin of conduction electrons is independent of the occupied valley [11,12]. This strong coupling between momentum and spin makes single-layer TMDs particularly appealing when compared to other valleytronics materials, such as Si [16] or graphene [17].

The MoS$_2$ optical response is dominated by two peaks at ~ 1.9 and 2.05 eV (denoted as A and B), related to interband optical transitions from the top of the spin split VB to the CB bottom [13]. These are strongly renormalized by excitonic effects, enhanced by the two dimensional (2D) nature of the material. The large spin-orbit interaction, combined with optical excitation by circularly polarized light, allows the photogeneration of electron (e) and hole (h) populations in the CB and VB, respectively, with $\sim 100\%$ spin and valley polarization [7,18], as measured by static helicity resolved photoluminescence (PL) experiments [18]. For this reason, a valley polarization lifetime ~ 1 ns was estimated for these materials [18]. Time-resolved PL experiments indicated that the lifetime of the valley polarization is limited by the fast photocarrier recombination, which occurs on the ps time scale [19]. This contrast between steady [18] and time-resolved PL measurements [19] can be reconciled by transient valley polarization experiments. Reference [20] reported a fast (i.e., few ps) exciton emission decay time, with a large circular polarization of the light emitted from the A excitonic transition. Helicity resolved pump-probe experiments also showed that the initial photoinduced valley polarization is rapidly quenched due to efficient intervalley scattering [21,22]. The relaxation dynamics in single TMD layers was also studied by transient Kerr rotation experiments with contradictory results [23–25]. In 1L-MoS$_2$ and WSe$_2$ an exciton valley decay time ranging from a few to tens ps was reported in Refs. [23,24], while
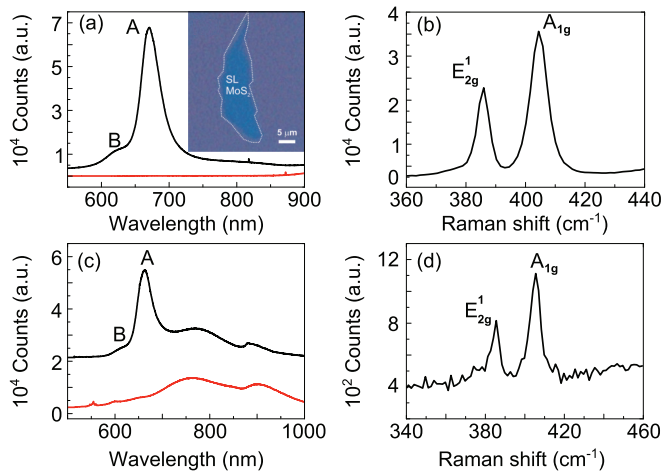
FIG. 1. (Color online) (a) PL and (b) Raman spectrum of 1L-MoS$_2$ on Si-SiO$_2$ (black line). (c) PL and (d) Raman spectrum of 1L-MoS$_2$ on fused silica. The red line is the PL spectrum of the substrate. Both sets of measurements are performed at room temperature for 514.5-nm excitation.

Ref. [25] measured a long-lived ns Kerr rotation dynamics at 5 K in 1L-MoS$_2$ and WS$_2$ and assigned this to spin/valley polarization transfer to the resident carriers.

Here, we measure the exciton valley relaxation dynamics in 1L-MoS$_2$ combining time-resolved Faraday rotation (TRFR) and time-resolved circular dichroism (TMCD). Both techniques allow for a temporal resolution of the order of hundreds fs. This is limited by the cross-correlation of pump and probe pulses, but is one order of magnitude better than time resolved PL experiments, where detection is performed by a streak camera [20]. We find that the temporal evolution of the Faraday angle, θ_F, has a double exponential decay, showing that the initial scattering of the photoinduced spin-polarized excitons from **K** to **K**$'$ is extremely quick ($\sim$200 fs). On a slower time scale, a residual component of the valley polarization, lasting $\sim$5 ps, is detected, in agreement with polarization resolved transient transmittivity measurements [22]. This fast valley polarization decay time is in good agreement with the time scale estimated by the Maialle-Silva-Sham e-h exchange interaction mechanism [26–29]. We also report the transient TRFR as a function of temperature and pump fluence. By increasing the temperature and the density of photoinduced excitons, we find that the valley decay time is strongly reduced. In particular, the quenching of the valley polarization for increasing exciton density is an indication of breakdown of the motional narrowing relation. This suggests that the depolarization dynamics in 1L-MoS$_2$ occurs with a linear dependence between valley and momentum relaxation times.

II. EXPERIMENT

MoS$_2$ flakes are produced by micromechanical cleavage of bulk MoS$_2$ onto Si + 285 nm SiO$_2$. 1L-MoS$_2$ flakes [Fig. 1(a)] are then identified by optical contrast, PL, and Raman spectroscopy [30,31]. Figure 1(b) shows a representative Raman spectrum of a flake used for our experiments, measured at

514.5 nm with a Renishaw microspectrometer. The position of the two main peaks is $\sim$385 and $\sim$404 cm^{-1}, indicating that this is 1L-MoS$_2$ [30–32]. Figure 1(c) plots the PL spectrum of the same flake measured at room temperature for 514.5-nm excitation. This consists of two bands at $\sim$1.85 and 1.98 eV, consistent with the A and B excitons in 1L-MoS$_2$ [33]. The selected 1L-MoS$_2$ flake is then moved by a wet-transfer technique based on a sacrificial layer of poly-methyl-methacrylate (PMMA) [34,35]. The polymer is deposited onto the flake by spin coating, followed by immersion in de-ionized water. Water intercalation at the PMMA-SiO$_2$ interface detaches the polymer film [34,35], with the 1L-MoS$_2$ flake attached on it. This is then moved onto a 100-μm-thick fused silica substrate and left to dry for a few hours. The fused silica substrate is particularly suitable for TRFR experiments since it is an isotropic material, without crystal orientation, and it does not exhibit birefringence [36]. PMMA is then removed by acetone, and the flake is released onto the fused silica [34,35]. A metal frame is then fabricated around the selected 1L-MoS$_2$ by photolithography, followed by thermal evaporation of 2 nm Cr and 100 nm Au. This ensures the same flake can be easily found for TRFR and TRCD measurements. To ascertain that no damage or changes are induced by the transfer process, this flake is further characterized after transfer and after the metal frame is defined. Figure 1 indicates no significant changes with respect to the initial sample prior to transfer.

TRFR experiments are performed as follows. A regeneratively amplified mode-locked Ti:sapphire laser with 1-kHz repetition rate drives two optical parametric amplifiers (OPAs). The output of the first OPA, circularly polarized and quasiresonant to the A exciton transition (650 nm) creates a spin- and valley-polarized e/h density with nonvanishing and well-defined orbital angular momentum. Contrary to previous Kerr rotation experiments on 1L-TMDs [23,24], the linearly polarized probe pulse is not degenerate with the pump, but it is centered at $\sim$700 nm, i.e. below the band gap. Both pump and probe pulses have a bandwidth $\sim$10 nm, corresponding to a temporal resolution $\sim$70 fs. The sample is positioned in a liquid-nitrogen cryostat and the temperature is checked by a thermocouple. The transmitted probe pulse passes through a Wollaston prism and it is focused on a couple of balanced photodiodes. The prism is rotated in order to equalize the probe intensities on the two photodiodes. The pump-induced signal imbalance is registered by a lock-in amplifier, locked to the pump 500-Hz modulation frequency.

TRCD experiments are performed with the same laser system by exciting the sample with a circularly polarized 650-nm pump. The probe is a white light continuum, in the 500–700 nm range, generated by a 2-mm-thick sapphire plate. The probe pulse is circularly polarized by a broadband quarter-wave plate. The probe spectrum is detected by an optical multichannel analyzer at the 1-kHz laser repetition rate and its differential transmission ($\Delta T/T$) is measured by chopping the pump at 500 Hz. Due to the use of a thick achromatic doublet to focus the probe beam, the TRCD temporal resolution, estimated from the rise time of the temporal traces, is slightly worse than for TRFR, being $\sim$200 fs for the entire spectral window of the probe beam.

III. RESULTS AND DISCUSSION

Because of the direct gap at the two degenerate valleys, the TRFR signal in MoS_2 is affected by two processes, depending on probe wavelength: (1) Pauli blocking, inhibiting the absorption of light with the same circular polarization of the pump [22]; (2) helicity-dependent light scattering from the photoexcited excitons [37]. In both cases, the imaginary part of the transient dielectric function assumes different values for opposite light helicities [11], so that the system displays asymmetric values of the phase accumulated by left- and right-circularly polarized light crossing the sample, resulting in the rotation of the polarization plane of the linearly polarized probe light. When the probe light is resonant with electronic transitions across the gap, the Faraday rotation is affected both by intervalley scattering and intravalley electron-spin relaxation [20]. In order to rule out the latter, we perform a two-color TRFR measurement in which the probe energy is deliberately tuned below the absorption edge. As far as electric dipole transitions are concerned, photons do not couple with the spin of charges, but only with their orbital degree of freedom [37]. Thus, the Faraday rotation associated with light scattering by the photoexcited charges can only derive from an unbalanced distribution of their orbital angular momentum projections. Since the orbital momentum of the carriers is associated with the valley degree of freedom, TRFR is mainly sensitive to intervalley and recombination dynamics, and it marginally depends on intravalley spin-flip processes.

Figure 2(a) plots the TRFR measurements at 77 K for left and right circularly polarized pump pulses. The change of sign of the signal with excitation helicity is a proof of the valley selectivity of the near-gap resonant transitions. As expected, TRFR with a linearly polarized pump pulse (grey curve) gives rise to a negligible signal because both valleys are equally populated. As highlighted in the inset of Fig. 2(b), $\theta_F(t)$ relaxes with two different time constants, dropping to 10% of the initial value after a few hundred fs, with a long-lived tail that decays on the ps time scale. The decay times are extracted by fitting the temporal trace with a double exponential decay convoluted with a Gaussian pulse with 70 fs full width at half maximum (FWHM), accounting for the instrumental response. The faster dynamics is $\tau_{\text{fast}} = 200 \pm 10$ fs while the slower is $\tau_{\text{slow}} = 4.8 \pm 0.2$ ps. The error bars are estimated from the fit of the two exponential decay functions to $\theta_F(t)$. We identify the rapid drop of the TRFR signal as a result of intervalley scattering of the photoexcited excitons. We note that the TRFR dynamics of a similar layered material (WSe_2), measured under the same experimental conditions [23], exhibits a monoexponential decay. This points to a more complex valley relaxation pathway for photoexcited excitons in MoS_2. Reference [26] suggested that the rapid decay of valley polarization in 2D TMDs is due to an *e-h* exchange mechanism. This process can be seen as a virtual annihilation of a bright exciton in one valley followed by the creation of an exciton in the opposite valley. Since the time scale associated with it is of the order of the inverse of the Coulomb *e/h* exchange interaction (i.e., on the order of hundreds of meVs [26]), the intervalley scattering time is estimated to be extremely fast (i.e., <20 fs) [26]. The temporal relaxation of the valley polarization after resonant excitation
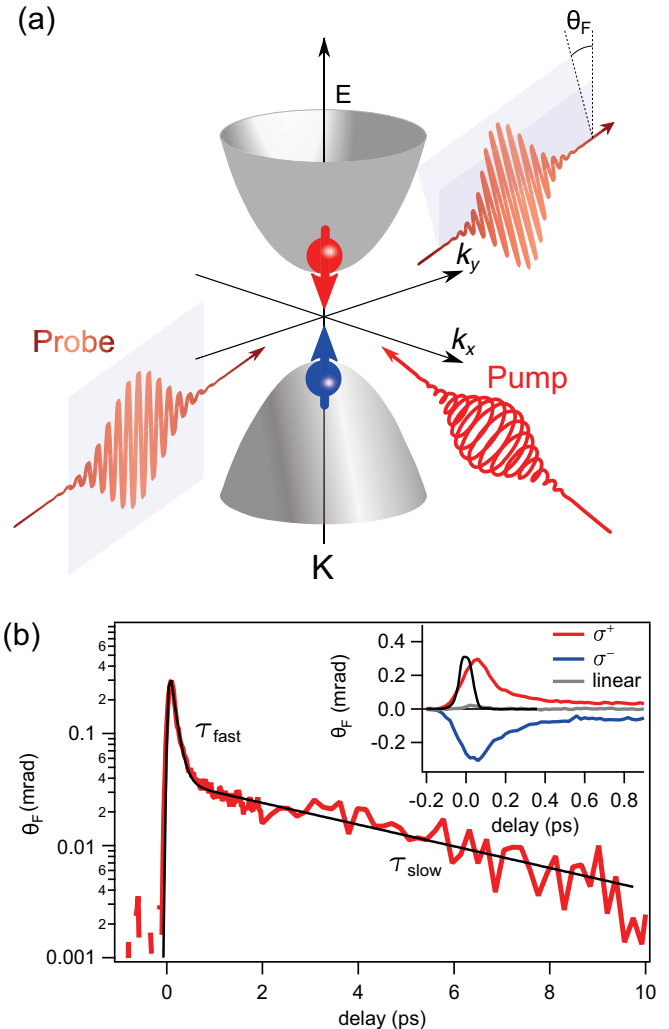

FIG. 2. (Color online) (a) Sketch of the TRFR experiment. The red and blue arrows represent the spin of the photoexcited *e* and *h*. (b) Temporal evolution of $\theta_F(t)$ in semilogarithmic scale in order to emphasize the biexponential character of the decay rate. The black continuous line is a double exponential fit to the data. The pump excitation is centered at 650 nm, while the probe wavelength $\lambda_{\text{pr}} = 700$ nm. The inset shows TRFR traces measured by exciting the sample with left and right circularly polarized pump pulses (red and blue curves, respectively) and a linearly polarized pump pulse (gray curve). All traces are measured at 77 K. The black line in the inset is the cross correlation between the pump and probe pulses. The FWHM of the cross correlation sets the temporal resolution of the TRFR experiment to 70 fs.

of the A exciton was estimated in Ref. [26] by solving the kinetic spin Bloch equations, neglecting the short-range part of the exchange interaction, and it is in good agreement with the measured fast decay of θ_F observed in our experiments. The small magnetic field associated with the long-range part of the exchange interaction is believed to be responsible for the slower decay, τ_{slow}, of the valley polarization [26,28].

The intervalley dynamics is further investigated by TRCD experiments. A circularly polarized pump, resonantly tuned with the optical gap, creates a spin polarized *e-h* pair in the **K** valley. The transient variation of transmittivity is
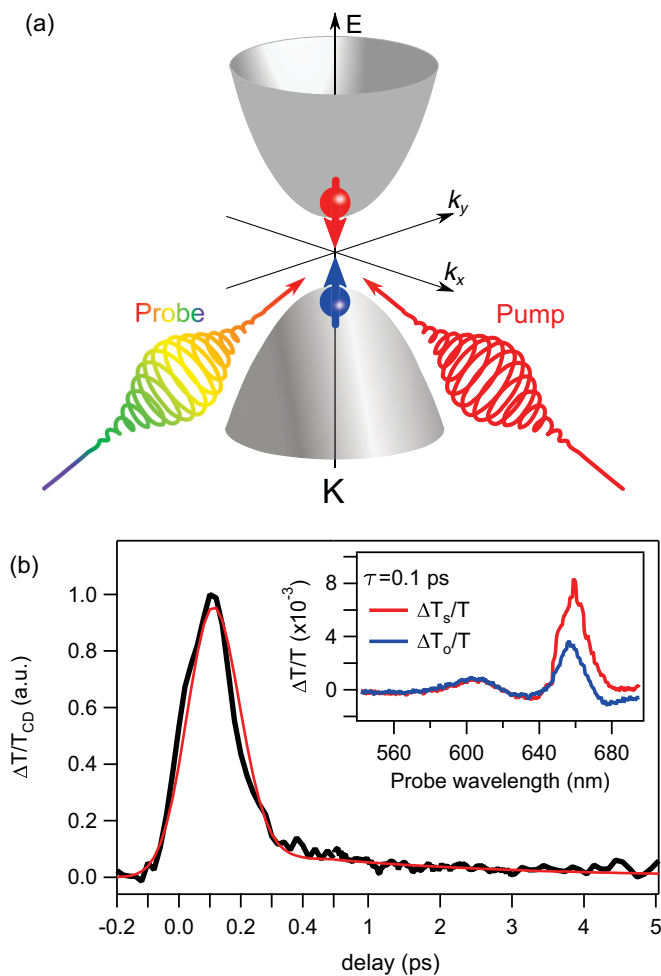
(a)

(b)

FIG. 3. (Color online) (a) Sketch of our TRCD experiments. (b) Black dots: difference between $\Delta T/T$ at 655 nm (peak of A exciton) measured by co- and countercircularly polarized probe pulses and normalized to unity. The time scale up to 500 fs is zoomed. Red solid curve: double exponential decay fit to the data. The inset plots $\Delta T/T$ traces at 77 K for co- and countercircularly polarized probe pulses (red and blue traces, respectively) at a delay time $\tau = 0.1$ ps. The circularly polarized narrow-band pump pulse is tuned to 650 nm, while the probe pulse covers a broad energy range between 500 and 700 nm.

measured by co- and countercircularly polarized broadband pulses probing respectively the temporal evolution of the photoexcited excitons within the same valley and the transient buildup of the population in $\mathbf{K}'$, due to intervalley scattering, as sketched in Fig. 3(a). Thus, the difference between the transient signals measured in the two configurations [i.e., when pump and probe pulses have the same (S) helicity or opposite (O) helicity] $\Delta T_{CD}/T(\lambda_{pr},t) = \Delta T_S/T(\lambda_{pr},t) - \Delta T_O/T(\lambda_{pr},t)$ is a direct probe of the relaxation dynamics of the valley polarization [21,22,38]. For both probe helicities, the transient optical response (blue and red traces in the inset of Fig. 3) is dominated by the A and B excitonic transitions at ∼655 and 605 nm [39]. The bleaching of the A excitonic transition in the $\Delta T_O/T(\lambda_{pr},t)$ spectrum is evidence of the fast charge delocalization due to intervalley scattering. This strong momentum

delocalization is consistent with the small radius of the TMDs' excitons, estimated to be ∼1 nm [40]. The anisotropy of the optical response is localized around the A exciton, while we do not observe any change of $\Delta T/T(\lambda_{pr},t)$ around B.

In order to study in more detail the time scale of the intervalley dynamics we report in Fig. 3 the difference between $\Delta T_S/T(\lambda_{pr},t)$ and $\Delta T_O/T(\lambda_{pr},t)$ integrated over the A excitonic transition. This trace decays exponentially with two different time scales, with a behavior analogous to the TRFR experiments. The fast decay constant is pulse width limited, while the slower dynamics lasts a few ps. Taking into account the lower time resolution of the TRCD experiments (∼200 fs), these time constants are in good agreement with τ_{fast} and τ_{slow} extracted from TRFR. Both experiments thus give us the same scenario for the decay of valley polarization in 1L-MoS$_2$ at 77 K: a fast initial decay on the 100-fs time scale, followed by a slow, ps recovery. Although an *e-h* recombination time of 4 ps was reported in Ref. [20] for 1L-MoS$_2$ at 4 K, first-principle calculations predict a linear increase of the intrinsic exciton radiative lifetimes at a rate of 1–10 ps/K [41]. Since our measurements are performed at 77 K and the *e-h* recombination is expected to be, at this temperature, at least one order of magnitude longer than the dynamics measured by TRCD and TRFR, we can neglect the exciton population decay contribution. Being $\Delta T_{CD}/T$ a direct measure of the difference between the spin- and valley-polarized exciton populations in the $\mathbf{K}$ and $\mathbf{K}'$ valleys, it is sensitive both to intervalley scattering and intravalley spin relaxation. However, within the time resolution of our TRCD experiments, we are not able to separately address the time scales of these two processes. We note that here we focus only on the study of the rapid intervalley scattering processes occurring on the 100-fs-to-ps time scales, and not the slow ns spin-relaxation dynamics of the resident carriers, as reported in Ref. [25] at 5 K for 1L-MoS$_2$, using transient Kerr spectroscopy. For our temperature range (77 K and higher) the long-lived spin polarization of the resident carriers is expected to become faster and likely to match the slower ps dynamics we measured [25].

The temperature dependence of the valley relaxation dynamics is then investigated by TRFR. Figure 4(a) plots the TRFR traces at different temperatures. Both τ_{fast} and τ_{slow} are sensitive to temperature, with a drop as the temperature increases, as in Figs. 4(b) and 4(c). This behavior was previously reported in Ref. [23] for WSe$_2$, and explained as due to the temperature variation of the momentum-dependent effective magnetic field, causing excitons precession, and consequent spin/valley polarization quenching. Reference [22] assigned the temperature dependence of the valley relaxation dynamics to scattering through the spin-degenerate Γ valley, which could become energetically favorable because the energy splitting between the electronic states at Γ and $\mathbf{K}$ is a few meVs for 1L-MoS$_2$ [12].

We then study the valley polarization at different exciton density regimes. The TRFR traces at different pump fluences (i.e., exciton densities) together with the extracted decay times are plotted in Fig. 4. We observe a pronounced decrease of both τ_{fast} and τ_{slow} as the number of the photoinjected excitons n_{ex} increases. For the TRFR traces with $n_{ex} > 20 \times 10^{12}$ cm^{-2}, it is difficult to deconvolve the fast decay dynamics, due to the limited temporal resolution. The exciton density dependence
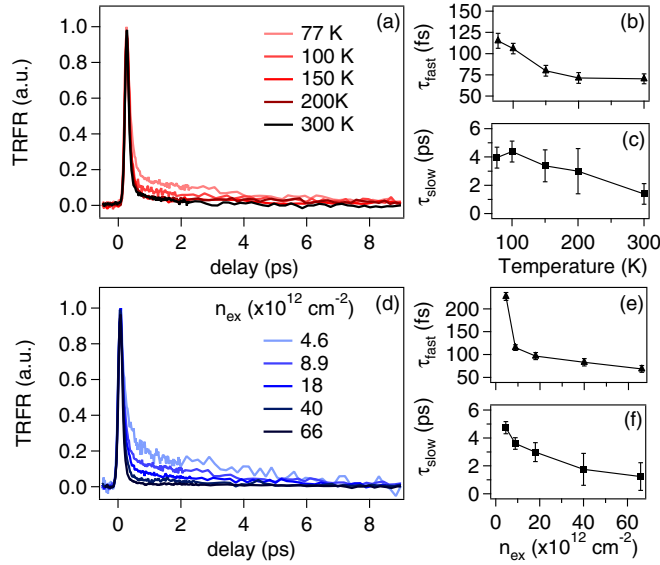
FIG. 4. (Color online) (a) Normalized TRFR dynamics in the 77–300 K range. (b),(c) Temperature dependence of the decay constants τ_{fast} and τ_{slow}. (d) Normalized TRFR dynamics at different exciton densities. (e),(f) Pump fluence/photoinduced excitons density dependence of τ_{fast} and τ_{slow}.

of the Faraday signal in Fig. 4 suggests an important role of excitonic effects in the intervalley scattering. This contrasts what is expected for spin relaxation in semiconductors in the motional narrowing regime [37] [i.e., $\langle\Omega^2(K)\rangle\tau \ll 1$] where $\langle\Omega^2(K)\rangle$ is the square of the Larmor frequency about the effective magnetic field associated with e-h exchange interactions, averaged over the entire exciton population, and τ is the momentum relaxation time. In this regime, before the spin of the excitons stops precessing around the effective magnetic field, the direction of the wave vector k is continuously changed by scattering with other carriers. As a consequence, the spin (valley) decay time $\tau_{s(v)}$ and the momentum relaxation time τ are inversely proportional: $1/\tau_{s(v)} \propto \tau$. τ results from the contribution of the $e-e$ scattering time, $\tau_{e\text{-}e}$, and the scattering time, τ_p, between electrons and other scattering centers, like defects and phonons ($1/\tau = 1/\tau_{e\text{-}e} + 1/\tau_p$) [37]. Since $\tau_{e\text{-}e}$ is expected to decrease at higher pump fluences, an increase of the exciton density would correspond to a shortening of the momentum scattering time and a consequent increase of the spin lifetime, exactly the opposite of Fig. 4. We stress that the measured $\tau_{\text{fast}}/\tau_{\text{slow}}$ dependence on n_{ex} also contrasts that predicted by the e-h exchange mechanism where, for lower τ, a slowing of the valley polarization is expected [26].

The strong quenching of the spin relaxation at increasing excitation fluence suggests that spin/valley relaxation

dynamics in MoS_2 is in a weak scattering regime where $\langle\Omega^2(K)\rangle\tau > 1$. Here the spin of the exciton precesses many times around the effective field, without undergoing scattering, and a linear relation between $\tau_{s(v)}$ and τ holds. Amongst all the mechanisms put forward to describe the spin/valley relaxation in 1L-TMDs, Elliot-Yafet (EY) [42] predicts a linear scaling between τ and $\tau_{s(v)}$ [43]. Reference [44] calculated an out-of-plane spin-relaxation time in 1L-MoS_2 of few ns (i.e., three orders of magnitude slower than our data). Such a slow relaxation time would be consistent with e/h spin out-of-plane components being good quantum numbers and conserved. Although EY in the intrinsic case cannot be responsible for the fast spin/valley relaxation dynamics, the presence of defects and out-of-plane flexural phonon modes could make the valley depolarization process more efficient [45]. A breakdown of the motional narrowing regime for increasing exciton densities was also reported in bulk GaAs [46] and 1L-WSe_2 [47].

IV. CONCLUSIONS

We characterized the valley relaxation dynamics in 1L-MoS_2 by combining TRFR and TRCD measurements. We detected a fast valley depolarization dynamics on two time scales ($\sim$100 fs and a few ps). We assigned the rapid intervalley exciton dynamics measured by TRFR, together with the fast buildup of the A exciton measured by opposite pump and probe helicity in TRCD, to electron-hole exchange interactions. We also investigated the temperature and excitation density dependence of the valley relaxations. The quenching of exciton valley polarization for increasing temperature is consistent with the increase of the exciton spin precession velocity around the effective magnetic field associated to the e/h interaction. We also observed that the intervalley scattering rate strongly increases at higher photoexcited exciton densities. This suggests that the valley relaxation processes in MoS_2 occurs in a regime where τ and $\tau_{s(v)}$ are proportional, paving the way to other possible extrinsic relaxation channels, like EY, involving the scattering with defects.

[1] I. Zutic, J. Fabian, and S. Das Sarma, Rev. Mod. Phys. **76**, 323 (2004).

[2] T. Yang, T. Kimura, and Y. Otani, Nat. Phys. **4**, 851 (2008).

[3] D. Ilgaz, J. Nievendick, L. Heyne, D. Backes, J. Rhensius, T. A. Moore, M. A. Niño, A. Locatelli, T. O. Mentes, A. V. Schmidsfeld, A. v. Bieren, S. Krzyk, L. J. Heyderman, and M. Kläui, Phys. Rev. Lett. **105**, 076601 (2010).

[4] V. E. Demidov, S. Urazhdin, H. Ulrichs, V. Tiberkevich, A. Slavin, D. Baither, G. Schmitz, and S. O. Demokritov, Nat. Mater. **11**, 1028 (2012).

[5] H. Dery, P. Dalal, L. Cywiski, and L. J. Sham, Nature (London) **447**, 573 (2007).

[6] F. Bottegoni, M. Celebrano, M. Bollani, P. Biagioni, G. Isella, F. Ciccacciand, and M. Finazzi, Nat. Mater. **13**, 790 (2014).

[7] D. Xiao, G.-B. Liu, W. Feng, X. Xu, and W. Yao, Phys. Rev. Lett. **108**, 196802 (2012).

[8] I. Zutić and P. E. Faria Junior, Nat. Nanotechnol. **9**, 750 (2014).

[9] A. C. Ferrari *et al.*, Nanoscale **7**, 4598 (2015).

[10] K. Roy, M. Padmanabhan, S. Goswami, T. P. Sai, G. Ramalingam, S. Raghavanand, and A. Ghosh, Nat. Nanotechnol. **8**, 826 (2013).

[11] K. Kośmider, J. W. González, and J. Fernández-Rossier, Phys. Rev. B **88**, 245436 (2013).

[12] A. Kormányos, V. Zólyomi, N. D. Drummond, P. Rakyta, G. Burkard, and V. I. Fal'ko, Phys. Rev. B **88**, 045416 (2013).

[13] K. F. Mak, C. Lee, J. Hone, J. Shan, and T. F. Heinz, Phys. Rev. Lett. **105**, 136805 (2010).

[14] G. Sallen, L. Bouet, X. Marie, G. Wang, C. R. Zhu, W. P. Han, Y. Lu, P. H. Tan, T. Amand, B. L. Liu, and B. Urbaszek, Phys. Rev. B **89**, 079903(E) (2014).

[15] H. Zeng, J. Dai, W. Yao, D. Xiaoand, and X. Cui, Nat. Nanotechnol. **7**, 490 (2012).

[16] D. Culcer, A. L. Saraiva, B. Koiller, X. Hu, and S. Das Sarma, Phys. Rev. Lett. **108**, 126804 (2012).

[17] A. Rycerz, J. Tworzydlo and C. W. J. Beenakker, Nat. Phys. **3**, 172 (2007).

[18] K. F. Mak, K. He, J. Shanand, and T. F. Heinz, Nat. Nanotechnol. **7**, 494 (2012).

[19] T. Korn, S. Heydrich, M. Hirmer, J. Schmutzler, and C. Schüller, Appl. Phys. Lett. **99**, 102109 (2011).

[20] D. Lagarde, L. Bouet, X. Marie, C. R. Zhu, B. L. Liu, T. Amand, P. H. Tan, and B. Urbaszek, Phys. Rev. Lett. **112**, 047401 (2014).

[21] Q. Wang, S. Ge, X. Li, J. Qiu, Y. Ji, J. Feng, and D. Sun, ACS Nano **7**, 11087 (2013).

[22] C. Mai, A. Barrette, Y. Yu, Y. G. Semenov, K. W. Kim, L. Cao, and K. Gundogdu, Nano Lett. **14**, 202 (2014).

[23] C. R. Zhu, K. Zhang, M. Glazov, B. Urbaszek, T. Amand, Z. W. Ji, B. L. Liu, and X. Marie, Phys. Rev. B **90**, 161302(R) (2014).

[24] G. Plechinger, P. Nagler, C. Schüller, and T. Korn, arxiv:1404.7674v3.

[25] L. Yang, N. A. Sinitsyn, W. Chen, J. Yuan, J. Zhang, J. Lou, and S. A. Crooker, Nat. Phys. **11**, 830 (2015).

[26] T. Yu and M. W. Wu, Phys. Rev. B **89**, 205303 (2014).

[27] M. Z. Maialle, E. A. de Andrada e Silva, and L. J. Sham, Phys. Rev. B **47**, 15776 (1993).

[28] M. M. Glazov, T. Amand, X. Marie, D. Lagarde, L. Bouet, and B. Urbaszek, Phys. Rev. B **89**, 201302(R) (2014).

[29] H. Yu, G.-B. Liu, P. Gong, X. Xu, and W. Yao, Nat. Commun. **5**, 3876 (2014).

[30] C. Lee, H. Yan, L. E. Brus, T. F. Heinz, J. Hone, and S. Ryu, ACS Nano **4**, 2695 (2010).

[31] X. Zhang, W. P. Han, J. B. Wu, S. Milana, Y. Lu, Q. Q. Li, A. C. Ferrari, and P. H. Tan, Phys. Rev. B **87**, 115413 (2013).

[32] R. S. Sundaram, M. Engel, A. Lombardo, R. Krupke, A. C. Ferrari, Ph. Avouris, and M. Steiner, Nano Lett. **13**, 1416 (2013).

[33] A. Splendiani, L. Sun, Y. Zhang, T. Li, J. Kim, C.-Y. Chim, G. Galli, and F. Wang, Nano Lett. **10**, 1271 (2010).

[34] F. Bonaccorso, A. Lombardo, T. Hasan, Z. Sun, L. Colombo, and A. C. Ferrari, Mater. Today **15**, 564 (2012).

[35] G. F. Scheneider, V. E. Calado, H. Zandbergen, L. M. K. Vandersypen, and C. Dekker, Nano Lett. **10**, 1912 (2010).

[36] http://refractiveindex.info/.

[37] M. I. Dyakonov and A. V. Khaetskii, in *Spin Physics in Semiconductors*, Springer Series in Solid-State Sciences, Vol. 157, edited by M. I. Dyakonov (Springer, Berlin, Heidelberg, 2008).

[38] C. Mai, Y. G. Semenov, A. Barrette, Y. Yu, Z. Jin, L. Cao, K. W. Kim, and K. Gundogdu, Phys. Rev. B **90**, 041414(R) (2014).

[39] S. Sim, J. Park, J.-G. Song, C. In, Y.-S. Lee, H. Kim, and H. Choi, Phys. Rev. B **88**, 075434 (2013).

[40] T. Cheiwchanchamnangij and W. R. L. Lambrecht, Phys. Rev. B **85**, 205302 (2012).

[41] M. Palummo, M. Bernardi, and J. C. Grossman, Nano Lett. **15**, 2794 (2015).

[42] P. G. Elliot, Phys. Rev. **96**, 266 (1954).

[43] H. Ochoa, A. H. Castro Neto, and F. Guinea, Phys. Rev. Lett. **108**, 206808 (2012).

[44] H. Ochoa and R. Roldan, Phys. Rev. B **87**, 245421 (2013).

[45] H. Ochoa, F. Guinea, and V. I. Fal'ko, Phys. Rev. B **88**, 195417 (2013).

[46] M. Krauss, H. C. Schneider, R. Bratschitsch, Z. Chen, and S. T. Cundiff, Phys. Rev. B **81**, 035213 (2010).

[47] T. Yan, X. Qiao, P. Tan, and X. Zhang, Sci. Rep. **5**, 15625 (2015).